analytical chemistry

Article

pubs.acs.org/ac

Velocity Profiles in Pores with Undulating Opening Diameter and Their Importance for Resistive-Pulse Experiments

Laura M. Innes,[†] Chin-Hsuan Chen,[‡] Matthew Schiel,[†,§] Matthew Pevarnik,[‡] Florian Haurais,[∥] Maria Eugenia Toimil-Molares,[∥] Ivan Vlassiouk,[⊥] Luke Theogarajan,[‡] and Zuzanna S. Siwy*[,†,§,#]

[†]Department of Physics and Astronomy, University of California, Irvine, California 92697, United States

[‡]Department of Electrical and Computer Engineering, University of California, Santa Barbara, California 93106, United States

[§]Department of Bioengineering, University of California, Irvine, California 92697, United States

[∥]Department of Materials Science, GSI Helmholtz Center for Heavy Ion Research, Darmstadt, Germany

[⊥]Oak Ridge National Laboratory, Bethel Valley Road, Oak Ridge, Tennessee 37831, United States

[#]Department of Chemistry, University of California, Irvine, California 92697, United States

Supporting Information

ABSTRACT: Pores with undulating opening diameters have emerged as an analytical tool enhancing the speed of resistive-pulse experiments, with a potential to simultaneously characterize size and mechanical properties of translocating objects. In this work, we present a detailed study of the characteristics of resistive-pulses of charged and uncharged polymer particles in pores with different aspect ratios and pore topography. Although no external pressure difference was applied, our experiments and modeling indicated the existence of local pressure drops, which modified axial and radial velocities of the solution. As a consequence of the complex velocity profiles, pores with undulating pore diameter and low-aspect ratio exhibited large dispersion of the translocation times. Distribution of the pulse amplitude, which is a measure of the object size, was not significantly affected by the pore topography. The importance of tuning pore geometry for the application in resistive-sensing and multipronged characterization of physical properties of translocating objects is discussed.

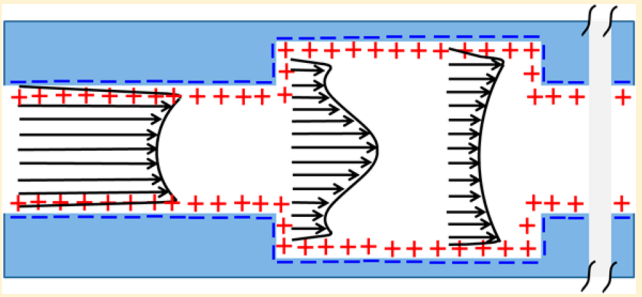

Transport of particles and molecules can be induced by an external electric field, pressure difference, or a combination of both. Passage of single particles through a pore causes a transient change of the pore resistance, called a resistive pulse.[1,2] The resistive pulse technique has been applied to detect a wide range of molecules and particles.[3−14]

When the species to be detected carries a net charge, its translocation in the external electric field can occur by electrophoresis. However, if the pore walls are charged, an applied voltage also causes electroosmotic flow of the whole solution. Thus, the translocation velocity is a superposition of electrophoretic and electroosmotic velocities.[15] Depending on the relative zeta potentials of the particles and the pore walls, the particles will follow either the direction of electroosmosis or electrophoresis.[16] The dependence of transport on particle charge has prompted the application of these electrokinetic phenomena for the detection of single molecules of DNA, proteins, viruses, and particles.[9−14,17,18]

The resistive pulse profile is intimately related to the velocity profile in the pore, which sometimes complicates its interpretation. There are two limiting cases where the velocity profile does not exhibit significant radial dependence: (1) Electrophoretic transport in an uncharged ideal cylindrically shaped pore subjected to sufficiently high voltages to make diffusion of the particles negligible.[15,19,20] (2) Electroosmotic flow in a cylindrical pore with charged walls and with a radius many times the thickness of the electrical double layer. Under these conditions, electroosmosis can be described by a plug-flow with constant velocity, decaying sharply to zero at the walls due to the nonslip boundary condition.[19−25] Most pore based detection platforms often operate at one of these limiting cases to ease interpretation of the resulting ion current profile. Undulating pores operate between these regimes and have emerged as a promising platform capable of probing not only size but also mechanical properties of translocating particles, as shown before with hydrogels.[26] The pores were also shown to enhance the speed of resistive-pulse analysis due to the ability to distinguish single versus few particles residing in the pore at the same time.[29] However, the pulse characteristics become quite complex and require detailed understanding of velocity profiles within the pore for proper extraction of material properties from the ion current signature.

Received: August 11, 2014
Accepted: September 23, 2014
Published: September 23, 2014

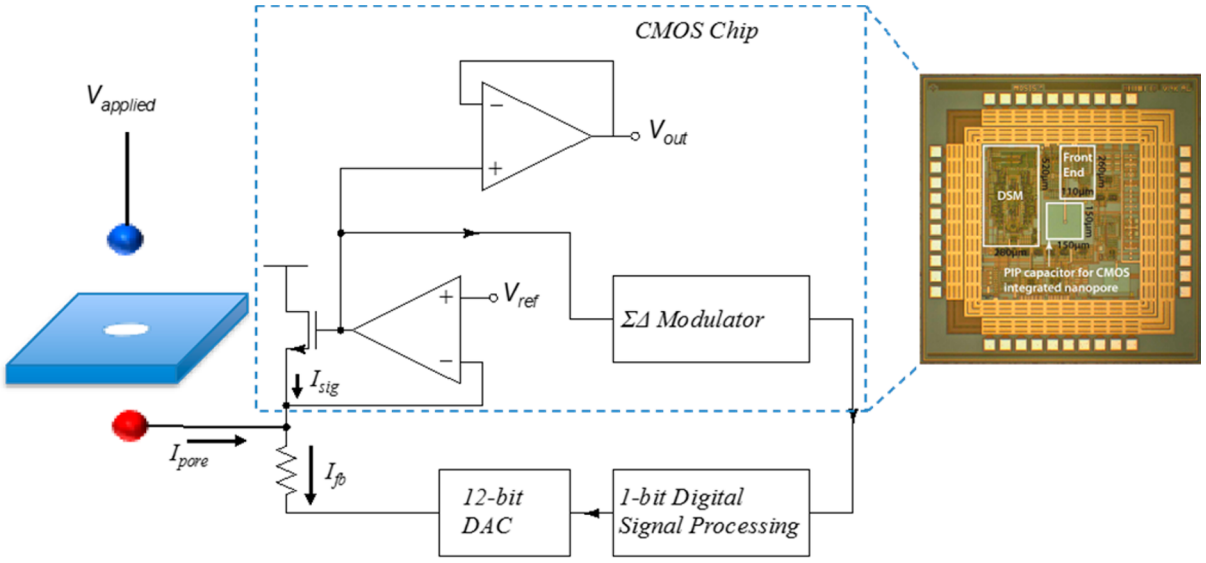

Figure 1. Schematic of the custom designed amplifier circuit. The circuit enables sensing small currents on a large baseline by utilizing baseline cancellation. In this topology the current is compressed using the transistor nonlinearity to prevent the circuit from saturating. The resulting signal is digitized and converted into a 1-bit digital signal using an oversampled A/D converter (ΣΔ). The baseline is extracted from the digital signal using digital signal processing and then converted back to an analog value via a D/A converter and fed back to the input canceling the baseline.[41]

We present here for the first time a detailed analysis of resistive pulses obtained with pores whose opening diameter varies along the pore axis. We performed both experiments and numerical modeling to elucidate the relationship between velocity profiles in the pores and the measured ion current. Single polymer pores with an average opening diameter between 1 and 15 μm were used to examine electrophoretic and electroosmotic transport of polystyrene particles. The pores were prepared in polyethylene terephthalate films (PET) by the track-etching technique and exhibit an undulating diameter along the pore axis.[27,28] Topography of each pore can be gleaned from the shape of resistive pulses.[26,29,30] When a particle passes through a region with a narrower local diameter, the current decrease will be larger compared to the case when the particle passes through a wider region. Large variations in the current amplitude within a resistive pulse indicate existence of large modulations of the pore diameter along the axis. In this manuscript, we provide experimental evidence that translocation times in pores with irregular longitudinal profiles are characterized by a larger variability compared to those in smoother pores. This effect is especially pronounced in structures with an aspect ratio less than four. The findings are in agreement with modeling showing the assumption of the plug-flow is not valid for pores characterized by a variable charge of the pore walls and/or variable cross-section area along the pore axis.[19,20,31−39] We modeled velocity and pressure profiles in pores with an undulating opening diameter by numerically solving the coupled Poisson-Nernst−Planck and Navier−Stokes equations. The modeling confirmed the velocity of fluid and consequently the velocity of the particles depend on both a radial position as well as the position along the pore axis. We believe this will allow the accurate interpretation of ionic current profiles obtained from pores with undulating diameters. Moreover, we have also shown the resulting inhomogeneous pressure drops and velocities do not adversely affect soft particles such as cells. Pores with undulating diameters have the potential to move the use of resistive pulse technique beyond mere sizing of particles, enabling the use of these structures for enhanced biomolecule detection.

EXPERIMENTAL SECTION

Preparation of Pores. Single pores in 12, 36, and 50 μm thick films of polyethylene terephthalate (PET) were prepared by the track-etching technique.[27] The films were irradiated with single energetic heavy ions (e.g., 11.4 MeV/u Au and U ions) at the UNILAC linear accelerator of the GSI Helmholtz Center for Heavy Ion Research in Darmstadt, Germany. Wet chemical etching of the films in 0.5 M NaOH, 70 °C, and in 2 M NaOH, 60 °C leads to preparation of pores with undulating pore diameter along the pore axis.[28,29] Both etching conditions were used in this project. The mean pore diameter was estimated from the current−voltage measurements performed in 1 M KCl and calculating the pore diameter from its conductance. Experiments presented here were performed with pores with an average opening diameter between 1 and 15 μm. The walls of track-etched PET pores contain carboxyl groups and are negatively charged at pH values above 3.8.[40]

Ion Current Recordings. Single pore membranes were placed between two chambers of a homemade conductivity cell filled with an aqueous solution of KCl either 0.1 M or 10 mM. Home-made Ag/AgCl electrodes were used in the measurements. Signals of ion current in time were recorded using two amplifiers. The first one, the commercially available Axopatch 200B (Molecular Devices, Inc.), is limited to measuring currents below 200 nA, thus was used for pores with an opening diameter smaller than ∼1.5 μm in 0.1 M KCl and smaller than 4 μm in 10 mM KCl. Ion currents through pores with a larger opening diameter was recorded using a custom designed CMOS chip based potentiostat capable of measuring sub-nA currents on a μA baseline.[41] A schematic of the circuit used is shown in Figure 1. Briefly the circuit enhances small signals by canceling the static baseline current utilizing a combination of nonlinear analog processing, oversampled A/D conversion, and digital signal processing. The removal of the baseline allows for a large dynamic range while simultaneously

dx.doi.org/10.1021/ac502997h | Anal. Chem. 2014, 86, 10445−10453

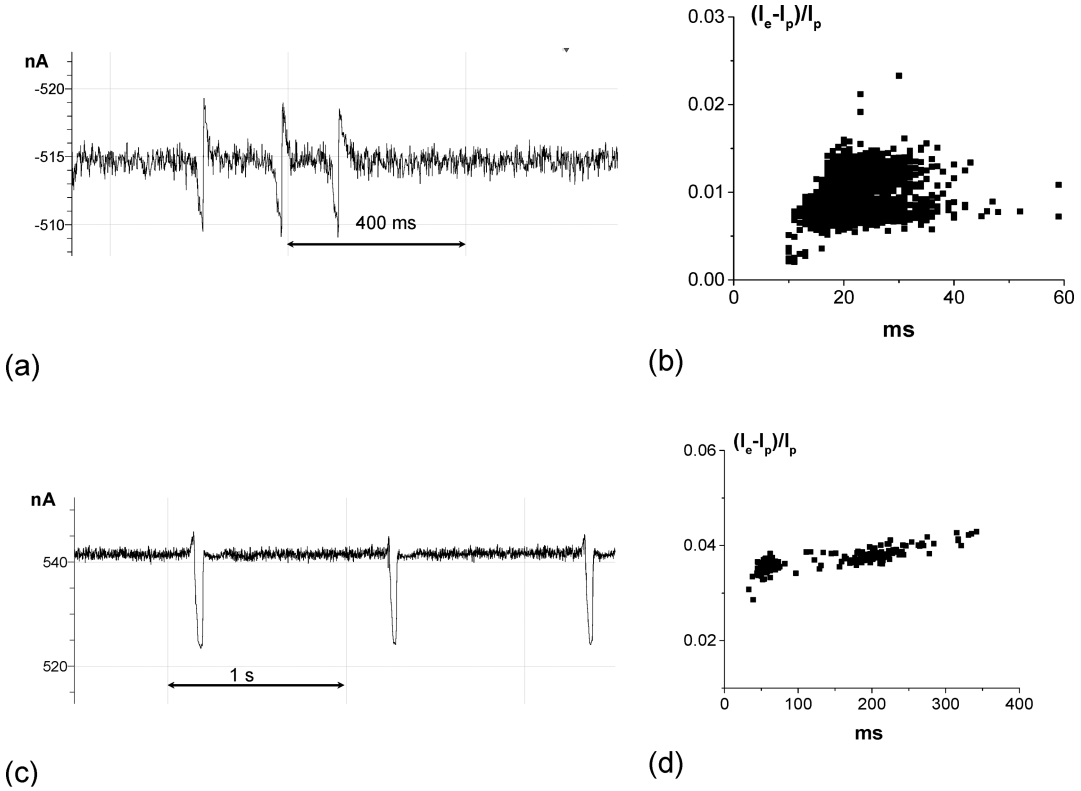

Figure 2. Example translocations of ~1 μm negatively charged polystyrene particles through a single 3 μm in diameter pore. The particles translocated in the direction of electrophoresis at −1 V (a) and electroosmosis at +1 V (c). (b,d) Corresponding scatter plots of the relative current change $(I_e - I_p)/I_p$ vs translocation time are shown. I_e and I_p indicate ion current through the pore without and with a particle, respectively. The recordings were performed in 0.1 M KCl, pH 10 with the custom designed amplifier; the commercially available amplifier Axopatch 200B cannot measure currents higher than 200 nA.

reducing the shot noise due to the baseline current further enhancing detection. The feedback also removes the slow baseline drift and any $1/f$ noise present in the signal up to the feedback filter bandwidth. Because of the nonlinear front-end and digital feedback loop, sudden changes, which normally would lead to saturation, can be quickly corrected.[41]

Ion current recordings were analyzed using Clampfit 10.4 and custom-written Matlab codes. An ion current pulse was defined as a current change equal to at least double root-mean-square of the baseline signal. Recordings at each condition, i.e., pore diameter, KCl concentration, and voltage, contained at least 200 events corresponding to passage of single particles.

Particles. Carboxylated polystyrene particles with a diameter between 410 nm and 5 μm and 400 nm poly(methyl methacrylate) (PMMA) particles were used in the experiments (Bangs Laboratories, Fisher, IN). For all recordings, a KCl solution (0.1 M or 10 mM, pH 10) with ~2×10^9 particles per mL was placed on one side of the membrane while the other side of the membrane was in contact with pure KCl of the same concentration as used for the particle solution. KCl solutions with particles contained 0.1% (v/v) Tween 80.

Metal Replica of the Channels. Porous membranes were obtained by chemical etching of 12 μm thick PET foils after heavy ion irradiation with 10^7 ions/cm^2 at the UNILAC linear accelerator at the GSI Helmholtz Center for Heavy Ion Research (Darmstadt, Germany). The chemical etching was performed in the same conditions as the single-pore samples, i.e., in 0.5 M NaOH at 70 °C. A thin Au layer was sputtered on one side of the membrane and electrochemically reinforced with copper. This layer acts as the cathode, while an Au wire acts as the anode in a two electrode setup. Au wires were electrodeposited using a gold sulfite-based bath at 50 °C, applying −0.7 V. The Au adopts the shape and size of the channels, thus scanning electron microscope (SEM) investigations on the wire morphology after PET dissolution in 9 M NaOH at room temperature yield information on the geometry of the channels investigated.

Cell Culture. Mice cells J774A.1 (ATCC TIB-67) were grown and maintained (5% CO_2, 37 °C) in DMEM (Life Technologies 10569-010) supplemented with 10% fetal bovine serum (Life Technologies 26140-079) and 2 mM L-glutamine (Life Technologies 25030-081). 60% J774A.1 confluent cells were trypsinized with 1% trypsin-EDTA (Life Technologies 15400-054), then counted and resuspended in PBS (Life Technologies 10010-023) to 1×10^4 cells/mL.

RESULTS AND DISCUSSION

Figure 2 shows example resistive pulses obtained with negatively charged polystyrene particles passing through a 3 μm diameter pore. In our electrode configuration, positive voltages indicate electroosmotic transport; for negative voltages, the particles translocated in the direction of electrophoresis. In this experiment, translocations were observed for both voltage polarities, albeit with different current profiles, indicating zeta potential of the particles was comparable to the zeta potential of the pore walls. Using the resistive pulse analysis relating the particle size with the amplitude of recorded pulses,[9,11] and including the access resistance of the system,[42] we found the average size of particles passing through the pore at negative voltages is ~1 μm, close to

dx.doi.org/10.1021/ac502997h | Anal. Chem. 2014, 86, 10445−10453

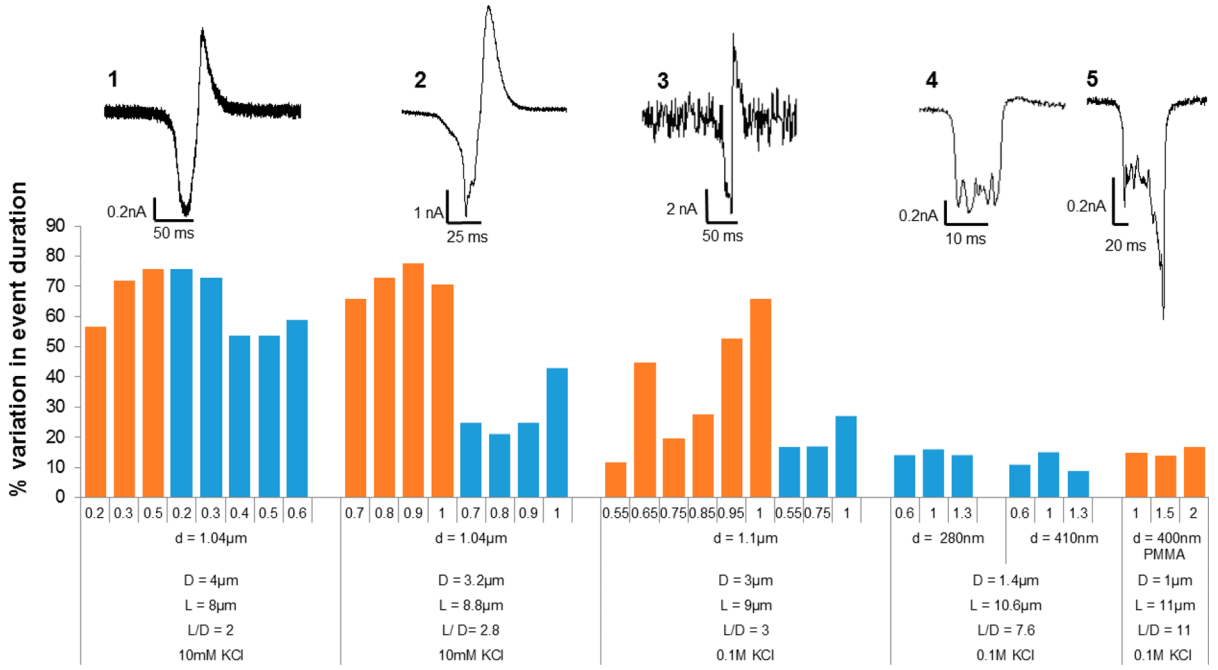

Figure 3. Analysis of translocation times of five different pores prepared in 12 μm thick PET films by the track-etching technique. Applied voltage in volts is indicated on the x-axis. The final length of the pores (L) is related with the pore opening diameter (D) due to etching away of the material. Pores with larger opening diameter are shorter. Particle diameter is marked as d. Orange and blue bars represent analysis of electroosmotic and electrophoretic transport of particles, respectively. Examples of resistive pulses for each pore are shown as insets. The percentage variability was calculated as the square root of variance divided by the average; both parameters were found based on histograms of translocation times as first two central moments. Ion current through pores 1, 2, 4, and 5 was performed with Axopatch 200B; pore 3 was studied using the custom built amplifier.

the nominal diameter given by the manufacturer, while for positive voltages the size is ~1.5 μm. Size of the particles determined by the resistive-pulse technique is known to be voltage-independent.[9,11] Thus, these experiments suggest larger particles are capable of being electroosmotically transported due to their lower overall surface charge density. Both dynamic light scattering and SEM imaging confirmed the sizes predicted using the resistive pulse.

Resistive pulses of the ~1 μm particles recorded for both voltage polarities were composed of a current decrease and a current increase. As previously discussed,[30,43] the double-peak character of the pulses results from the transient modification of ionic concentrations at the pore entrance and exit caused by the translocating particles. The ionic enhancement occurs when a negatively charged particle is at the pore end in contact with a positively biased electrode. Consequently, resistive-pulses of particles moving in the electrophoretic direction consist of a current decrease followed by a positive peak. Particles whose transport is dominated by electroosmosis translocate for the opposite voltage polarity, and their resistive pulses begin with a current increase.[30]

Scatter plots of relative current change, $(I_e - I_p)/I_p$ where I_e and I_p are currents without and with a particle, respectively, and pulse duration of the two recordings shown in Figure 1 suggest for this pore the electroosmotic translocations are characterized by a larger variability of translocation times compared to the electrophoretic transport. The dispersion of event durations cannot be attributed to size variations of particles, since the distribution of relative current change due to electroosmotic transport was similar to electrophoresis-dominated transport (Supporting Information, Figure S1). The observation on large variability of the translocation times was reported before in resistive-pulse experiments in which particles passed through a pore by externally applied pressure difference.[44,45] Radial position of the particles with respect to the pore axis was predicted to greatly affect the translocation time and have smaller influence on the pulse amplitude. The large variability of translocation times in our experiments suggests the particles can indeed follow different trajectories when passing through the pores.

In order to facilitate comparison of experiments performed at different voltages, pores, and particles, all recordings were analyzed using histograms of resistive pulse durations. For each recording at least 200 events were analyzed. The histograms allowed us to find weighted average and variance for each parameter and calculate the percentage variation in the determination of average translocation time. Because of the large number of pulses analyzed in each voltage, the standard error of the variance does not exceed 10%. Figure 3 summarizes the analysis for the recordings performed with ~1 μm particles and 3 μm pore at different voltages (pore 3) and compares the findings with analysis of two other, independently prepared pores with an average opening diameter of 3.2 and 4 μm (pores 1−2). The analysis suggests that translocation times in all the studied pores were characterized by dispersions significantly higher compared to our earlier experiments with particles.[29,46] This effect was especially pronounced in cases when the transport occurred in the direction of electroosmosis.

The three pores were prepared by etching heavy ion irradiated polymer films with an initial thickness of 12 μm. Since the opening diameter was a few micrometers, the etching process also led to a significant thinning of the films and lowering of the pore aspect ratio to ~3. Our earlier experiments were performed with pores prepared in the same type of films, but their diameter was always sub-1.5 μm assuring an aspect ratio above 6.[26,29,30] Figure 3 compares, in addition, the

dx.doi.org/10.1021/ac502997h | Anal. Chem. 2014, 86, 10445−10453

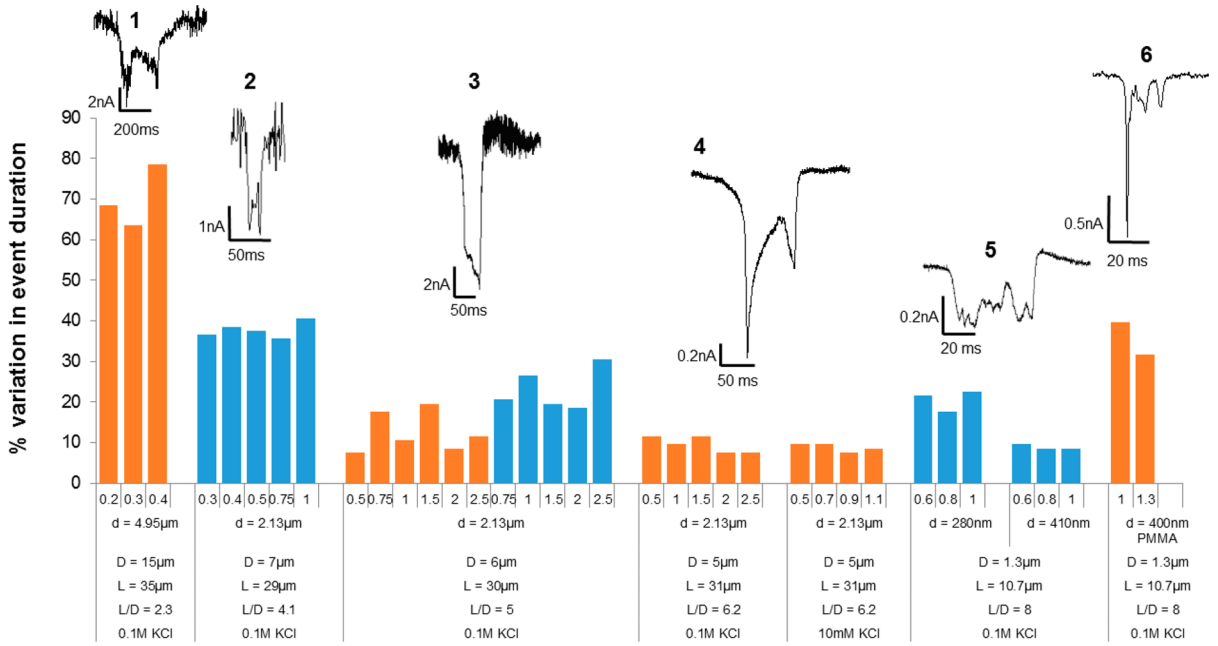

Figure 4. Dispersion of translocation times of six pores with varying opening diameter, length, and topography. Applied voltage in volts is indicated on the *x*-axis. Examples of resistive pulses for each pore are shown as insets. *L*, *D*, and *d* stand for pore length, pore diameter, and the particle diameter. Orange and blue bars represent analysis of electroosmotic and electrophoretic transport of particles, respectively. Recordings in pores 1−4 in 0.1 M KCl were performed using the custom built amplifier. Data in 10 mM KCl in pore 4 and all recordings in pores 5−6 were obtained using Axopatch 200B.

dispersion of translocation times in the three short pores (pores 1−3) with two long pores (pores 4,5) with an opening diameter of ∼1 μm and length of ∼11 μm used to observe electrophoretic transport of 410 nm carboxylated polystyrene particles and electroosmotic translocation of 400 nm PMMA uncharged particles. Translocation times in the longer pores were characterized by low dispersion typically not exceeding 20%.

The analysis in Figure 3 suggests pores with low, less than 4, aspect ratios producing wide distributions of translocation times. This result, at least partly, could be explained by the existence of various paths a particle can take when approaching and translocating a pore.[47] As the next step, we wanted to understand whether pore roughness, observed as ion current fluctuations within resistive pulse, influence the distribution of event durations as well. Additional resistive-pulse experiments were therefore performed using pores with an average opening diameter between 1.3 and 15 μm and length between 11 and 35 μm.

Figure 4 summarizes variability of translocation times recorded for six additional pores. In general, pores with aspect ratio above 5 produced significantly lower dispersion of translocation times compared to short structures. For longer pores, the dispersion reached ∼30% only when the pore was characterized with large modulations of the pore opening diameter and contained large cavities such that the current in the pulse approached the baseline current (pore 6, 1.3 μm in diameter, Figure 4). The data for 2 μm particles passing through 5, 6, and 7 μm in diameter pores with length ∼30 μm indicate the translocation time varies more significantly in wider pores. A similar conclusion can be drawn noticing a larger dispersion in the recordings with 280 nm particles versus 410 nm particles electrophoretically passing through a 1.3 μm pore (pore 5 in Figure 4). The bar graph also shows analysis of 5 μm particles translocating a low aspect ratio pore with an opening diameter of 15 μm (pore 1); the data support our earlier conclusion (Figure 3) that short pores produce a wide distribution of event durations.

Roughness of PET pores prepared by the track-etching technique was confirmed by us directly via an imaging metal replica of multipore membranes.[28,29] This approach provided a convenient way of investigating topography of many pores prepared in the same way. Here we use the same template approach to understand whether pore roughness increases with the increase of the etching time. Figure 5 shows representative wires electrodeposited in originally 12 μm thick PET

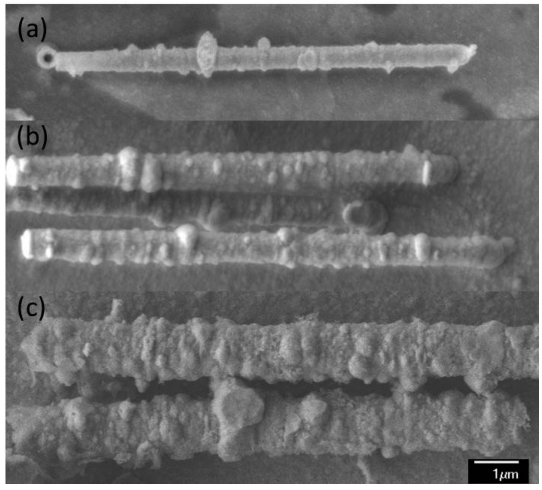

Figure 5. SEM images of representative gold wires electrodeposited in PET membranes containing 10^7pores/cm^2. The PET membranes were obtained by irradiating originally 12 μm thick PET films and etching in 0.5 M NaOH, 70 °C for (a) 136 min, (b) 180 min, and (c) 300 min. Average wire diameters are 490 nm (a), 660 nm (b), and 1230 nm (c).

dx.doi.org/10.1021/ac502997h | *Anal. Chem.* 2014, 86, 10445−10453

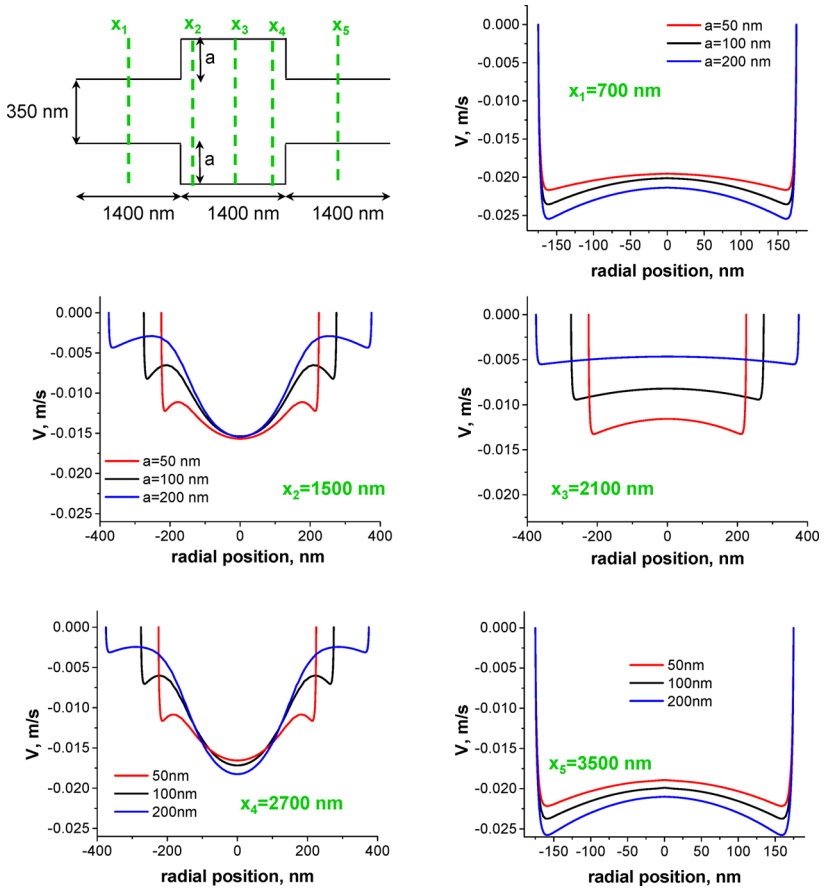

Figure 6. Radial profiles of axial velocity at five different positions along an axis of a 4.2 μm long pore with undulating opening diameter and surface charge density of −0.5 e/nm^2. Bulk electrolyte concentration was set as 10 mM KCl. The modeling was performed by numerically solving coupled Poisson−Nernst−Planck and Navier−Stokes equations. The modeled structure is schematically shown in the upper left panel (not to scale).

membranes with average diameters of (a) 490 ± 40, (b) 660 ± 30, and (c) 1230 ± 70 nm. The images display the overall cylindrical geometry of the wires (i.e., the channels) together with the irregular profile along the channel axis, attributed to the layered structure of the pristine PET foils.[28] Analysis of the shape of wires (n > 20) of each sample revealed that the number of large protuberances defined as a diameter increase larger than 15% from the average value and does not depend on the etching time. Longer etching times, however, promote formation of additional smaller irregularities and longitudinal widening of the large cavities (Figure 5). The range of opening diameters investigated by the metal replica method is narrower than the range of pore openings used in the resistive-pulse experiments due to limited availability of thicker polymer films irradiated with many ions.

In order to interpret the resistive-pulse data and dispersion of translocation times, we considered properties of electroosmostic velocity of fluid in a pore with an undulating opening diameter. Continuity equation imposes the fluid velocity in narrower regions must be higher than in the wider parts of the pore. As a consequence, a wider zone pulls the liquid from the narrower region where a lower pressure is established. Thus, transport of particles through a charged pore with undulating opening diameter has to be considered as an electrokinetic flow with a superimposed pressure difference.[19,20] Interestingly, local pressure drops and position dependent velocity distribution were predicted theoretically and observed experimentally before in an electroosmotic flow in a smooth, cylindrical capillary with inhomogeneous zeta potential.[34−36] The visualization of the flow in this system was achieved by using an optically activated fluorescent dye of caged 5-(and 6)-carboxy-Q-rhodamine.[35]

Figure 6 shows the cross-section of a pore system that was numerically modeled to understand the radial and axial dependence of electroosmosis induced fluid velocities in a pore with undulating opening diameter. A positively biased electrode was placed at the right opening of the pore, thus in this configuration, the electroosmotic fluid flow is directed from right to left. Velocity profile and ion current were modeled by numerically solving coupled Poisson−Nernst−Planck and Navier−Stokes equations.[26,48] Achieving convergent solutions required a large computational power and a pore with length of 4.2 μm was considered to make the computation tractable while providing the requisite physical insight. The pore contained two narrower entrances with an opening diameter of 350 nm and a wider cavity with a tunable diameter between 450 and 750 nm. We also performed modeling of a 0.9 μm long structure consisting of three zones with opening diameters of 350, 550, and 350 nm, respectively. The pores carried a homogeneous surface charge density of −0.5 e/nm^2. All calculations were performed in 10 mM KCl as bulk electrolyte.

Figure 6 presents radial profiles of fluid velocity at five different positions along the axis of the 4.2 μm long pore. In the narrower regions, the velocity is relatively flat with a local minimum at the pore axis and maxima close to the pore walls. Similar profiles were reported for a smooth cylindrical pore

dx.doi.org/10.1021/ac502997h | Anal. Chem. 2014, 86, 10445−10453

with fluid flow occurring under the opposing influence of electroosmosis and pressure difference.[49,50] Velocity profiles in the wider, middle region of the pore are however more complex and dependent on the axial position. Both ends of the wider region are characterized by a radial velocity profile such that the maximum velocity occurs at the pore axis, and two local minima are present at a small distance from the pore walls. Velocity in the radial direction in the zone between the walls and distance a is a few times lower than at the pore center; the difference is more pronounced for larger undulations. For the undulation a = 200 nm, the liquid even 100 nm away from the walls is almost stalled. The middle of the wider pore region (x_3 in Figure 6) has a qualitatively similar profile as the one observed in the narrower regions (x_1 and x_5).

Velocity profiles observed at the cross sections x_2 and x_4 in Figure 6 are well-known in macroscopic systems and are explained by a boundary layer at the walls, which is unable to follow sharp turns and corners.[39,51,52] In systems with high Reynolds numbers, flow separation can be observed where the boundary layer moves in the opposite direction to the main fluid flow through the center of the channel. In our system, the velocity did not change the sign but significantly decreased over an extended radial region. The modeling also confirmed formation of local pressure differences, whose magnitudes were the largest for the largest diameter undulations (Figure 7).

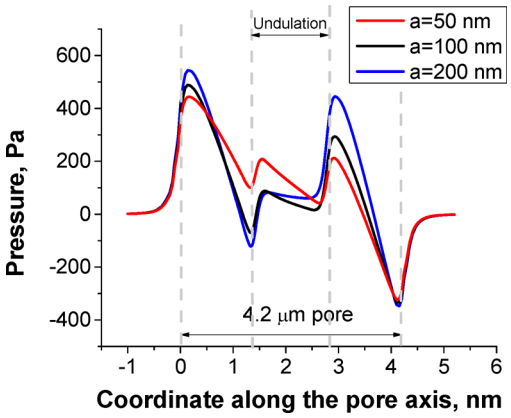

Figure 7. Modeled pressure profiles along the pore axis of a pore with undulating diameter whose scheme is shown in Figure 6. The value of "a" indicates the magnitude of the step size change of the opening diameter of the middle region (Figure 6).

We also modeled velocity profiles in a shorter pore with an aspect ratio of ~3 (Figure 8). The absolute values of velocities are higher than in the 4.2 μm long pore due to a larger electric field set by the same potential difference of 1 V. Qualitatively, the velocity profile in the narrower region is similar to what was obtained for a longer pore (Figure 6). Since the step in the pore opening diameter (a = 100 nm) is comparable to the length of each pore segment (300 nm), fluid velocity in the wider region never reaches the flatter profile but contains the three extrema at all positions along the axis (x_2 in Figure 8d).

The obtained velocity profiles suggest that depending on the path a particle takes when passing through a pore, it can move with significantly different velocities resulting in different translocation times. The large radial velocity gradients are especially pronounced in the wider regions of a pore where the velocity at the pore axis can be several times larger than closer to the walls. In pores with many undulations created during prolonged etching, a large portion of the pore length can feature the more complex velocity profiles, which could indeed lead to dramatically different translocation times. Translocation times in addition might be affected by a trajectory of the particle close to the pore entrance, which determines the radial position in the beginning of the translocation process.[53] In a given pore, a smaller particle can probe more radial positions with different velocities leading to wider distribution of translocation times compared to larger particles.

Since the pores exhibit pressure and velocity profiles that are axial position dependent, it raises the possibility that the pores could significantly deform a soft translocating particle. Previously, pores with undulating opening diameters were used to detect transport of 300 nm in diameter deformable hydrogels.[26] Negatively charged hydrogels passed through sub-1 μm polymer pores in the direction of electroosmosis, and the developed inhomogeneous pressure distribution led to the hydrogels' collapse and possible dehydration. In this study we decided to determine whether pressure and velocity gradients in larger pores are sufficient to deform microscopic objects such as biological cells.

Figure 9 shows example electroosmotic passage of single mouse J774A.1 macrophage cells from reticulum cell sarcoma present in a solution together with 10^8/mL 5 μm negatively charged polystyrene particles. Because of the large size difference, passage of the cells could be easily distinguished among the translocation of the smaller particles. Resistive pulses of both the polystyrene particles and the cells consisted of two downward peaks suggesting the pore contained a larger cavity in the middle. The pulses of hard polystyrene particles were symmetric suggesting the constriction zones at the two pore entrances had similar opening diameters. The two peaks in pulses corresponding to the cells were however characterized by significantly different amplitudes suggesting the intrinsically built in pressure differences in a pore with undulating opening diameter could have deformed the cells; the second, smaller current decrease could therefore correspond to an effectively smaller cell. Our experiments therefore suggest that in order to elucidate mechanical properties of passing objects it is important to know the pore topography and to perform comparative studies with hard spheres. Interpretation of resistive-pulses created by hydrogels was also facilitated by comparison with pulses of polystyrene particles.[26]

CONCLUSIONS

We have presented resistive-pulse experiments with polystyrene particles passing through polymer pores by electrophoresis and electroosmosis. Because of the undulating opening diameter of the pores, electroosmotic velocity exhibits complex dependence on both the radial and axial positions. As a result, pores with finite surface charges and large longitudinal irregularities produce wide distributions of translocation times even in cases when the particles move in the direction of electrophoresis. The velocity variations are even more pronounced in pores with low aspect ratios and pores where the properties of the boundary layer close to the walls dominate velocity profile over an extended length of the pore.

Pores with undulating opening diameter however provide an important analytical tool due to the presence of intrinsic pressure drops at the boundaries between regions with a different opening diameter. Our experiments with biological cells presented here as well as earlier experiments with hydrogels[26] suggest the developed pressure gradients of a few

dx.doi.org/10.1021/ac502997h | Anal. Chem. 2014, 86, 10445−10453

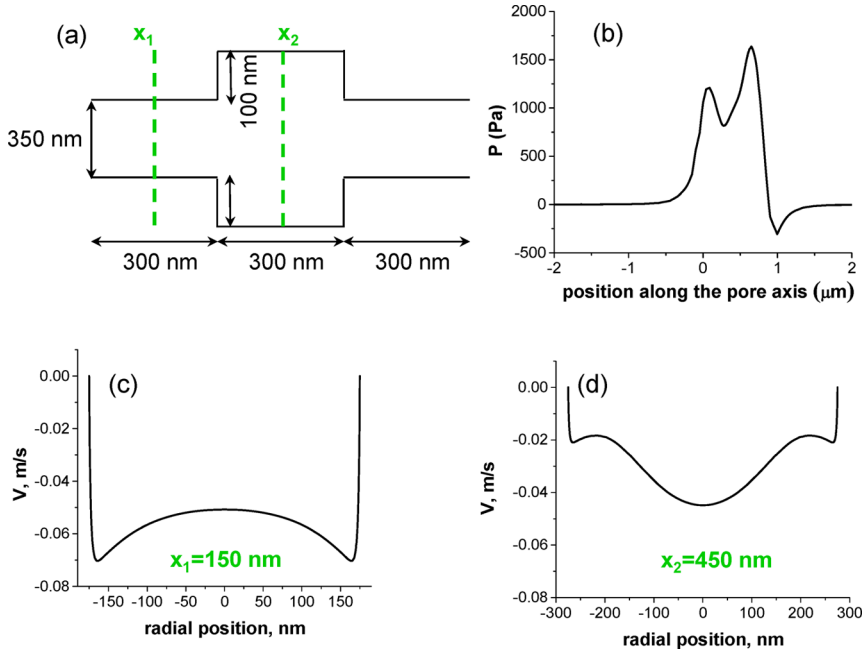

Figure 8. (a) Scheme of a 900 nm long pore modeled by the Poisson−Nernst−Planck and Navier−Stokes equations in 10 mM KCl, with 1 V applied across the pore with a positively biased electrode on the right-hand side. (b) Pressure profile along the pore axis. The pore openings are at the position 0 and 0.9 μm. (c,d) Radial velocity profiles at two positions along the pore axis, as indicated in part a.

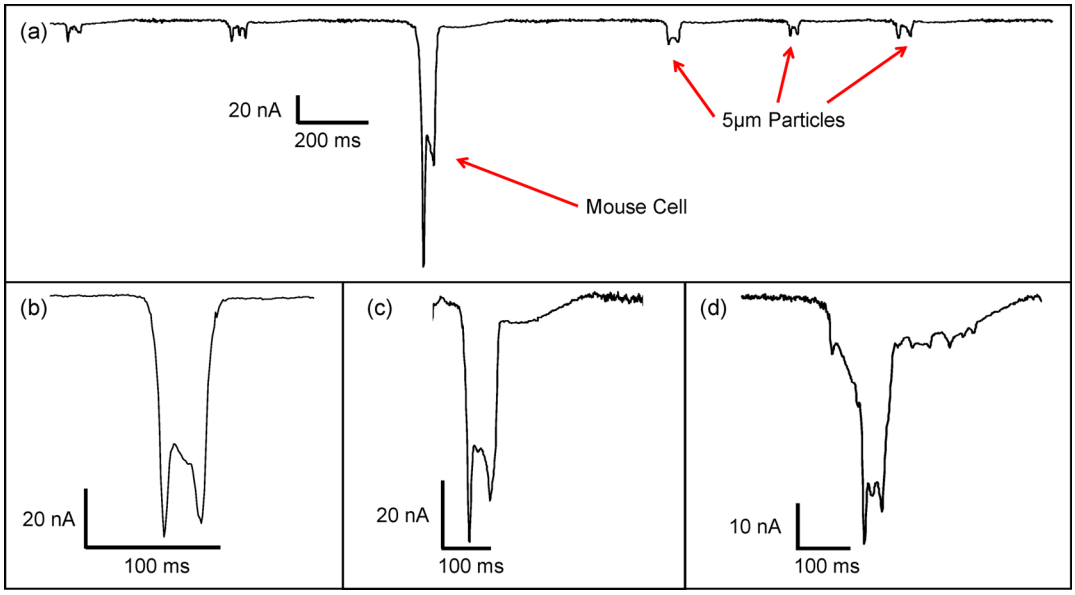

Figure 9. (a) Ion current recording through a 15 μm in diameter pore in the presence of 5 μm in diameter polystyrene particles and mouse J774A.1 macrophage cells. (b−d) Examples of single cell passage from the same recording are shown. Solution on one side of the membrane contained 0.1 M KCl with 10^8 particles/cm^3 and ~2×10^4 cells spiked into a 2 mL solution. Both the particles and the cells passed in the direction of electroosmosis at 0.4 V. The recordings were performed with the custom built amplifier.

hundreds of Pa are sufficient to deform the passing objects and might inform about their mechanical properties. Pores with undulating opening diameter have the potential of extending the resistive-pulse technique beyond sizing and provide a high-throughput technique of probing mechanical properties of meso and micro-objects.

In order to mitigate the issue of large dispersion of translocation times, we performed analysis of the dependence of the velocity profiles on the length of pore undulations. We have found that when the wider regions are sufficiently long, the velocity profiles in all regions reach similar characteristics and exhibit small radial variability; such pores are expected to produce narrow distribution of translocation times and a good estimate of the object electrokinetic velocity. Our experiments and analysis point therefore to the importance of the pore topography and geometry for the outcome of resistive-pulse experiments. In our future studies we plan to prepare metal replica of single-pore samples used for resistive-pulse experiments to be able to correlate the resistive-pulse shape and modeled velocity profiles with exactly known pore geometry.

dx.doi.org/10.1021/ac502997h | *Anal. Chem.* 2014, 86, 10445−10453

■ ASSOCIATED CONTENT

Supporting Information

Analysis of amplitude of resistive pulses for all pores presented in the main manuscript. This material is available free of charge via the Internet at http://pubs.acs.org.

■ AUTHOR INFORMATION

Corresponding Author

*E-mail: zsiwy@uci.edu. Phone: (949) 824-8290.

Author Contributions

The manuscript was written through contributions of all authors. All authors have given approval to the final version of the manuscript.

Notes

The authors declare no competing financial interest.

■ ACKNOWLEDGMENTS

Irradiation with swift heavy ions was performed at the GSI Helmholtz Center for Heavy Ion Research, Darmstadt, Germany. The authors acknowledge the use of the Biological Nanostructures Laboratory within the California NanoSystems Institute, especially Dr. Lior Dassau, supported by the University of California, Santa Barbara, and the University of California, Office of the President. This research was supported by the National Science Foundation (Grant CHE 1306058) and the National Institutes of Health, through the NIH Director's New Innovator Award Program (Grant 1-DP2-OD007472-01).

■ REFERENCES

(1) Bayley, H.; Martin, C. R. *Chem. Rev.* **2000**, *100*, 2575−2594.
(2) Henriquez, R. R.; Ito, T.; Crooks, R. M. *Analyst* **2004**, *129*, 478−482.
(3) Kasianowicz, J. J.; Brandin, E.; Branton, D.; Deamer, D. W. *Proc. Natl. Acad. Sci. U.S.A.* **1996**, *93*, 13770−13773.
(4) Venkatesan, B. M.; Bashir, R. *Nat. Nanotechnol.* **2011**, *6*, 615−624.
(5) Cherf, G. M.; Lieberman, K. R.; Rashid, H.; Lam, C. E.; Karplus, K.; Akeson, M. *Nat. Biotechnol.* **2012**, *30*, 344−348.
(6) Manrao, E. A.; Derrington, I. M.; Laszlo, A. H.; Langford, K. W.; Hopper, M. K.; Gillgren, N.; Pavlenok, M.; Niederweis, M.; Gundlach, J. H. *Nat. Biotechnol.* **2012**, *30*, 349−353.
(7) Movileanu, L. *Soft Matter* **2008**, *4*, 925−931.
(8) Coulter, W. H. *Means for Counting Particles Suspended in a Fluid.* U.S. Patent 2,656,508, 1953.
(9) DeBlois, R. W.; Bean, C. P.; Wesley, R. K. A. *J. Colloid Interface Sci.* **1977**, *61*, 323−335.
(10) Berge, L. I.; Feder, J.; Jøssang, T. *Rev. Sci. Instrum.* **1989**, *60*, 2756−2763.
(11) DeBlois, R. W.; Bean, C. P. *Rev. Sci. Instrum.* **1970**, *41*, 909−916.
(12) DeBlois, R. W.; Wesley, R. K. A. *J. Virol.* **1977**, *23*, 227−233.
(13) Harms, Z. D.; Mogensen, K. B.; Nunes, P. S.; Zhou, K.; Hildenbrand, B. W.; Mitra, I.; Tan, Z.; Zlotnick, A.; Kutter, J. P.; Jacobson, S. C. *Anal. Chem.* **2011**, *83*, 9573−9578.
(14) Zhou, K.; Li, L.; Tan, Z.; Zlotnick, A.; Jacobson, S. C. *J. Am. Chem. Soc.* **2011**, *133*, 1618−1621.
(15) Schoch, R. B.; Han, J.; Renaud, P. *Rev. Mod. Phys.* **2008**, *80*, 839−883.
(16) Firnkes, M.; Pedone, D.; Knezevic, J.; Döblinger, M.; Rant, U. *Nano Lett.* **2010**, *10*, 2162−2167.
(17) Wanunu, M. *Phys. Life Rev.* **2012**, *9*, 125−158.
(18) Howorka, S.; Siwy, Z. S. *Chem. Soc. Rev.* **2009**, *38*, 2360−2384.
(19) Ghosal, S. *J. Fluid Mech.* **2002**, *459*, 103−128.
(20) Ghosal, S. *Electrophoresis* **2004**, *25*, 214−228.
(21) Rice, C. L.; Whitehead, R. *J. Phys. Chem.* **1965**, *69*, 4017−4024.
(22) Kirkby, B. J.; Hasselbrink, E. F., Jr. *Electrophoresis* **2004**, *25*, 187−202.
(23) Pennathur, S. *Lab Chip* **2008**, *8*, 383−387.
(24) Chang, H.-C.; Yeo, L. Y. *Electrokinetically Driven Microfluidics and Nanofluidics*; Cambridge University Press: Cambridge, U.K., 2010.
(25) Keh, H. J.; Liu, Y. C. *J. Colloid Interface Sci.* **1995**, *172*, 222−229.
(26) Pevarnik, M.; Schiel, M.; Yoshimatsu, K.; Vlassiouk, I.; Kwon, J. S.; Shea, K. J.; Siwy, Z. S. *ACS Nano* **2013**, *7*, 3720−3728.
(27) Fleischer, R. L.; Price, P. B.; Walker, R. M. *Nuclear Tracks in Solids: Principles and Applications*; University of California Press: Berkeley, CA, 1975.
(28) Müller, S.; Schötz, C.; Picht, O.; Sigle, W.; Kopold, P.; Rauber, M.; Alber, I.; Neumann, R.; Toimil-Molares, M. E. *Cryst. Growth Des.* **2012**, *12*, 615−621.
(29) Pevarnik, M.; Healy, K.; Toimil-Molares, M. E.; Morrison, A.; Létant, S. E.; Siwy, Z. S. *ACS Nano* **2012**, *6*, 7295−7302.
(30) Menestrina, J.; Yang, C.; Schiel, M.; Vlassiouk, I.; Siwy, Z. S. *J. Phys. Chem. C* **2014**, *118*, 2391−2398.
(31) Hu, Y.; Werner, C.; Li, D. *Anal. Chem.* **2003**, *75*, 5747−5758.
(32) Hu, Y.; Xuan, X.; Werner, C.; Li, D. *Microfluid. Nanofluid.* **2007**, *3*, 151−160.
(33) Wang, M.; Wang, J.; Chen, S. *J. Comput. Phys.* **2007**, *226*, 836−851.
(34) Anderson, J. L.; Idol, W. K. *Chem. Eng. Commun.* **1985**, *38*, 93−106.
(35) Herr, A. E.; Molho, J. I.; Santiago, J. G.; Mungal, M. G.; Kenny, T. W.; Garguilo, M. G. *Anal. Chem.* **2000**, *72*, 1053−1057.
(36) Ren, L.; Li, D. *J. Colloid Interface Sci.* **2001**, *243*, 255−261.
(37) Yang, D.; Liu, Y. *Colloids Surf., A* **2008**, *328*, 28−33.
(38) Cho, C.-C.; Chen, C.-L.; Chen, C.-K. *ASME J. Fluids Eng.* **2013**, *135*, 021301 (1−11).
(39) Cummings, E. B.; Griffiths, S. K.; Nilson, R. H.; Paul, P. H. *Anal. Chem.* **2000**, *72*, 2526−2532.
(40) Ermakova, L. E.; Sidorova, M. P.; Bezrukova, M. E. *Colloid J.* **1998**, *52*, 705−712.
(41) Chinhsuan, C.; Yemenicioglu, S.; Uddin, A.; Corgliano, E.; Theogarajan, L. *Engineering in Medicine and Biology Society (EMBC), 2013 35th Annual International Conference of the IEEE*, 2013; pp 164−167.
(42) Hall, J. E. *J. Gen. Phys.* **1975**, *66*, 531−532.
(43) Lan, W.-J.; Kubeil, C.; Xiong, J.-W.; Bund, A.; White, H. S. *J. Phys. Chem. C* **2014**, *118*, 2726−2734.
(44) Berge, L. I.; Jøssang, T.; Feder, J. *Meas. Sci. Technol.* **1990**, *1*, 471−474.
(45) Saleh, O. A.; Sohn, L. L. *Rev. Sci. Instrum.* **2002**, *73*, 4396−4398.
(46) Schiel, M.; Siwy, Z. S. *J. Phys. Chem. C* **2014**, *118*, 19214−19223.
(47) Adams, R. B.; Gregg, E. C. *Phys. Med. Biol.* **1972**, *17*, 830−842.
(48) White, H. S.; Bund, A. *Langmuir* **2008**, *24*, 2212−2218.
(49) Dutta, P.; Beskok, A.; Warburton, T. C. *Numer. Heat Transfer, Part A: Appl.* **2002**, *41*, 131−148.
(50) Dutta, P.; Beskok, A. *Anal. Chem.* **2001**, *73*, 1979−1986.
(51) Bluestein, D.; Niu, L.; Schoephoerster, R. T.; Dewanjee, M. K. *Ann. Biomed. Eng.* **1997**, *25*, 344−356.
(52) Forrester, J. H.; Young, D. F. *J. Biomech.* **1970**, *3*, 297−305.
(53) Chein, R.; Dutta, P. *Colloids Surf. A* **2009**, *341*, 1−12.